DEM modelling to assess internal stability of gap-graded assemblies of spherical particles under various relative densities, fine contents and gap ratios

Mehrdad Ahmadi
PhD Applicant
Department of Infrastructure Engineering, The University of Melbourne
Parkville, Victoria, Australia 3010
Email: mehrdada@student.unimelb.edu.au

Thomas Shire
Lecturer
James Watt School of Engineering, The University of Glasgow
Glasgow G12 8QQ, United Kingdom
Email: Thomas.Shire@glasgow.ac.uk

Amirhassan Mehdizadeh
Research Fellow
Department of Infrastructure Engineering, The University of Melbourne
Parkville, Victoria, Australia 3010
Email: amirhassan.mehdizadeh@unimelb.edu.au

Mahdi Disfani (Corresponding Author)
Senior Lecturer
Department of Infrastructure Engineering, The University of Melbourne
Parkville, Victoria, Australia 3010
Email: mahdi.miri@unimelb.edu.au

Corresponding Author:
Mahdi Disfani
Department of Infrastructure Engineering, The University of Melbourne
Parkville, Victoria, Australia 3010
Email: mahdi.miri@unimelb.edu.au, Phone: +61383445972

Abstract

It is believed that the relative density (D_r) can affect the internal stability of the gap-graded soils and hence the erosion of their fine particles (i.e. susceptibility to suffusion). This paper investigates the influence of D_r on the contribution of fine particles on soil fabric. A new procedure is proposed to produce samples with target D_r using the discrete element method (DEM). DEM simulations were carried out using spherical particles. Particulate scale analysis of variation of stress reduction factor (α^{DEM}), the evolution of contact type and fine particle coordination number (Z^{fine}) with D_r reveals how D_r affects packing stability. The results show that packings with a fine content of 35% and the gap ratio in a range of 4-7 are in the transitional zone in which they are unstable initially and become internally stable as D_r increases. The behaviour of gap graded soil in the transitional zone is governed by fine-coarse contacts, but fine-fine contacts dominate the behaviour when soil becomes internally stable. Both α^{DEM} and Z^{fine} are reliable parameters in determining internal stability of gap graded soils. Finally, the correlation between the results and macro-scale matrix phase diagrams confirms the validity of micro-scale information to describe the underlying phenomenon.

Keywords: Relative Density; Gap-graded Soil; Discrete Element Method; Internal Stability; Contact Type; Internal Erosion

1. Introduction

Internal erosion is one of the major threats to water management structures such as embankment dams and is responsible for almost 50% of dam failures [1]. Internal erosion can occur in different forms including backward erosion, contact erosion, concentrated leak and suffusion [2]. Suffusion is the selective migration of non-plastic fine particles through the voids of soil made mainly of coarse particles due to seepage forces [2–9]. Soils which are susceptible to suffusion are termed "internally unstable". Suffusion, as a complex phenomenon, starts with the detachment of loose fine particles and continues with their transport under seepage flow which sometimes coincides with self-filtering (clogging) in voids [3,10,11]. Therefore, the local particle size distribution, porosity and hydraulic conductivity may change as suffusion occurs. This can also lead to a change in the mechanical properties of the soil as a result of a change in its microstructure [3,11].

According to Garner and Fannin [12], a combination of material susceptibility, critical hydraulic load and critical stress condition determines whether suffusion will occur or not. The material susceptibility depends on both geometric and stress criteria. The geometric criterion compares constriction sizes within the pore network with a representative fine particle size [13,14]. Constriction sizes can change as gap ratio, fine content, effective stress, particle shape and relative density vary [15]. Gap ratio (GR) and the fine content (FC) are defined as the size ratio between smallest coarse and largest fine particles, and the fine fraction by percent mass, respectively. The stress criterion considers the transmitted effective stress to the fine and coarse particles which are directly related to the fine fraction in the soil particle size distribution curve and stress state. If coarse particles form a continuous contact network (the fine fraction is not sufficient to fill pores between coarse particles), fine particles will carry little or zero stress and

will be prone to being washed out by seepage force. However, fine particles will actively participate in the stress transmitting matrix if coarse particles are floating in the finer matrix [2]. If geometric and stress criteria are met, then the critical hydraulic condition determines the possibility of the occurrence of suffusion [13].

The influence of the fine content and gap ratio on the erodibility of fine particles and their contribution to the soil skeleton has been widely studied both numerically and experimentally [13,16–23]. However, the impact of relative density on how fine particles contribute to the soil structure is still not thoroughly understood.

To experimentally quantify the compactness state of a soil sample, the relative density index is extensively used [24–26]. The relative density (Eq. 1) compares the current void ratio of the sample to the maximum and minimum void ratios [25,26].

$$D_r = \frac{e_{max} - e}{e_{max} - e_{min}} \qquad (1)$$

where, e_{max}=maximum void ratio of the sample at loosest state, e_{min}=minimum void ratio of the sample at the densest state and e=current void ratio of the sample.

Depending on the fine content and gap ratio, the relative density may affect the stress fabric of gap graded soils. The influence of the relative density on gap graded soil packing can be investigated through the evolution of contacts, contact forces and fine particle contribution to the soil stress fabric.

Following Skempton and Brogan [27], the stress reduction factor, α (Eq. 2), was proposed to show the average effective stress transmitted by the fine fraction with respect to the total effective stress applied to the soil.

$$\alpha = \sigma'_f / \gamma' z \qquad (2)$$

where σ'_f = transmitted vertical effective stress to the fine fraction; α=stress reduction factor; γ'=buoyant unit weight; z=soil depth. Skempton and Brogan [27] and Li and Fannin [28]

subsequently showed that critical hydraulic gradient ($i_c = \alpha \times \gamma' / \gamma_w$ [27]) for suffusion is directly proportional to α in internally unstable soils.

The influence of relative density on suffusion has been investigated in experimental studies. Ke and Takahashi [20] conducted a series of experiments on gap graded soils with GR=6.7 to study the influence of relative density in two extreme conditions: loose and dense. They found that back-calculated α at critical hydraulic gradient (i_c) decreased when fine content increased from 14.3% to 25%. In fact, this trend could continue until the threshold fine content (the fines content at which the fines completely fill the voids, and therefore the stress transmitted in the fines increases) is reached [20]. Erodibility of fine particles decreased (i.e. the back-calculated α increased) above the threshold fine content. The threshold value for erodible fine content was calculated to be 37% by Ke and Takahashi [20]. It was understood that the relative density had a minimal influence on erodibility of fine particles and the back-calculated α in the gap graded soil with a high gap ratio and fine content less than the threshold value.

Ahlinhan and Achmus [29] found that the back-calculated α for internally unstable soils was insensitive to the relative density, whereas soils on the borderline of internal stability (according to the Kenny and Lau [30] geometric criterion) were highly sensitive to relative density. This was in agreement with findings presented by Indraratna et al. [23].

Current literature [19,20,31–33] indicates that fine content can also affect the mechanical behaviour of gap graded soil. The influence of suffusion on the cyclic resistance and liquefaction potential of internally unstable soil was studied by Mehdizadeh et al. [31]. It was suggested that the erosion of fine particles made the soil samples more cyclic resistant regardless of the erosion progress. They believed it was due to a better interlocking of the coarse particles at very small strains as a result of suffusion and readjustment of soil structure.

The critical literature review of current experimental studies [20,23,29,33] suggests that the relative density can affect internal stability and the mechanical behaviour of non-plastic gap graded soil at the macro-scale. Due to the discrete nature of granular material, macro-scale behaviour is controlled by micro-scale interactions of the packing. The discrete element method (DEM) [34] is a micro-scale numerical modelling tool. It provides particulate scale information which is not always possible to capture in physical experiments [17,35–43]. Hence, further investigations need to be conducted at the micro-scale in DEM to develop a better understanding of the underlying phenomenon impacting experimental findings conducted at a macro-level.

Shire et al. [13] used DEM to study the influence of relative density on the soil fabric with a wide range of gap ratios and fine contents. However, in their study, the relative density was only described in qualitative terms, loose, medium and dense, and linking the degree of relative density to material behaviour was not attempted. To control sample density, different coefficients of friction (μ) were assigned to the generated cloud of non-overlapping particles. Then, particle assemblies were isotropically compressed to the mean normal stress of p'=50 kPa to produce loose ($\mu = 0.3$), medium ($\mu = 0.1$) and dense ($\mu = 0$) samples. Regardless of the relative density, it was found that the majority of fine particles were under-stressed and sat loose inside voids for the mixtures with fine content of less than 24% and a high gap ratio. This means the fine fraction was not adequate to fill the voids between coarse particles, so relative density did not improve the contribution of the fine particles to the soil fabric. When the fine content was higher than 35%, fine particles were found to separate coarse particles and actively contribute to the soil fabric. They concluded that when the fine content is in the range of 24-35%, relative density improves the contribution of fine particles to the load-bearing mechanism.

To investigate the influence of relative density on soil fabric in DEM quantitatively, samples with maximum and minimum void ratios should be produced. Unlike physical experiments, there is no standardized procedure for producing samples with minimum and maximum void ratios in DEM. Garcia and Bray [44] proposed an approach to measure the loosest state (e_{max}) by mimicking air pluviation. For the densest state (e_{min}), a sample was uniaxially compressed to 1MPa in a frictionless condition. The friction coefficient for dense and loose samples were 0 and 0.5, respectively.

This paper defines an alternative method to quantify the relative density of gap graded granular packings in DEM based on the modification of interparticle friction coefficient under constant confining pressure. Then the influence of the relative density on the fabric of granular assemblies with a wide range of fine content and gap ratio is quantitatively explored through micro-scale parameters. The stress reduction factor (α), coordination number and evolution of different contact types are considered as micro-scale parameters. The simulation of gap-graded materials requires large numbers of particles to achieve a representative elementary volume (REV) and contact detection is less computationally efficient. This means that simulations of gap-graded materials are computationally expensive. Perfectly spherical particles are computationally efficient and were therefore used in this study. However, they are an idealization of real granular materials and this is recognized as a limitation of this study. In particular, perfect spheres can freely rotate while, due to the angular shape particles and existence of interlock between particles, real granular assemblies are known to have a degree of resistance to rotation.

2. Modelling

Discrete Element Method was originally developed by Cundall and Strack [34]. It has been extensively used to investigate the granular material fabric at a particulate scale. The

simulations here were conducted in PFC3D [45]. A cloud of non-plastic, polydisperse non-overlapping particles was generated in a cubic geometry with rigid walls. The Hertz-Mindlin contact model was used to capture particle interactions.

Table 1 shows the simulation input parameters. Gravity was also neglected to avoid segregation, anisotropy and inhomogeneity in the packing. Gap graded particle size distributions were produced by generating the required number of particles in fine and coarse fraction through power-law distribution function at random positions.

Table 1 DEM simulation input parameters

Parameter	Unit	Value
Particle-Particle Contact Poisson's Ratio, ν	—	0.2
Particle-Particle Contact Shear Modulus, G	GPa	29.2
Particle Local Damping Coefficient	—	0.3
Particle Density, ρ	Kg/m^3	2500
Particle Shape	—	Perfect Sphere
Particle-Wall Contact Poisson's Ratio, ν	—	0.2
Particle-Wall Contact Shear Modulus, G	GPa	29.2
Wall Stiffness	—	Rigid
Timestep	s	4.04e-08
Loosest State Particle-Particle Coefficient of Friction, μ_{max}	—	1
Densest State Particle-Particle Coefficient of Friction, μ_{min}	—	0
Particle-Wall Coefficient of Friction, μ	—	0

Following Shire et al. [13], the fine particles' contribution to the soil stress matrix can be quantified through DEM stress reduction factor (α^{DEM}). The average index of the contribution of the fine fraction to the soil stress transmitting matrix, α^{DEM}, is calculated using (Eq. 3) [13]. The α^{DEM} is defined in terms of the volumetric mean normal stress of fine fraction, p'_{fine} (Eq. 4), and the volumetric mean normal stress of the soil sample, p' (Eq. 5).

$$\alpha^{DEM} = \frac{p'_{fine}}{p'} \tag{3}$$

$$p'_{fine} = \frac{\sum_{p=1}^{N_{p,fine}} v_p \times \frac{\sigma_{1(p)}+\sigma_{2(p)}+\sigma_{3(p)}}{3}}{\sum_{p=1}^{nN_{p,fine}} v_p} \tag{4}$$

$$p' = \frac{\sum_{p=1}^{N_p} v_p \times \frac{\sigma_{1(p)}+\sigma_{2(p)}+\sigma_{3(p)}}{3}}{\sum_{p=1}^{N_p} v_p} \tag{5}$$

where: $N_{p,fine}$: number of fine particles; v_p: particle volume; $\sigma_{1(p)}$, $\sigma_{2(p)}$ and $\sigma_{3(p)}$: principal particle normal stresses and N_p: the number of particles in the soil sample.

Two extreme fabrics of *(i)* overfilled and *(ii)* underfilled can be identified in gap graded soils [46] (Figure 1). In the overfilled state, fine and coarse particles carry effective stress approximately at the same level (FC≥35%; $\alpha^{DEM} > 0.8$). In this case, the majority of fine particles have a strong contribution to the soil stress transmitting matrix. Hence, the fine fraction cannot be eroded easily by seepage flow. In the underfilled state at the other extreme, the soil stress transmitting matrix is mainly made of coarse particles (FC≤24%; $\alpha^{DEM} < 0.4$) and hence, the poorly-stressed fine fraction can be washed out by seepage flows [13].

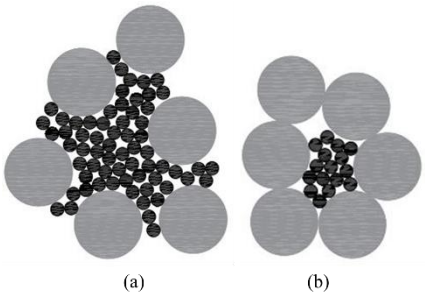

Figure 1. (a) Overfilled and (b) underfilled soil samples

2.1.Relative Density Procedure

To study the effect of relative density on the contribution of fine particles to the load-carrying mechanism, maximum and minimum void ratios of the packing need to be quantified. Standard methods exist to experimentally measure e_{min} (e.g. ASTM D4253 [25]) and e_{max} (e.g. ASTM D4254 [26]). According to ASTM D4253, e_{min} is measured by placing soil in a standard cylindrical metal mould, which is placed on a shaking table with a 14 kPa surcharge applied. According to ASTM D4254, e_{max} is measured by pouring soil into the mould by holding the pouring device about 13 mm above the soil surface in a spiral path. Once e_{min} and e_{max} are

158 known, a soil sample with the target relative density can be prepared using accepted preparation
159 methods such as under-compaction [47].

160 e_{min} and e_{max} should be quantified in DEM to investigate the influence of relative density on
161 gap graded materials at a particulate scale. However, it is very difficult (if not totally
162 impossible) to mimic experimental measurement of relative density in DEM directly. In order
163 to prevent segregation and produce a homogenous sample, gravity is often neglected. To
164 achieve the densest and loosest sample states in the DEM, the friction coefficient (μ) is
165 modified. Considering DEM limitations and influential parameters such as sample preparation,
166 particle shapes and confining pressures on e_{min} and e_{max}, an alternative method, appropriate for
167 DEM, is proposed here.

168 The friction coefficient of 0 was used to prepare a sample in DEM at the densest state in
169 previous studies [13,17,38,48]. However, there is no agreement between previous studies in
170 DEM in defining e_{max}. Minh and Cheng [38] used the friction coefficient of μ=0.5 and
171 compressed the sample isotropically to the mean normal stress of p' = 100 kPa. Shire at al. [13]
172 assigned μ=0.1 and μ=0.3 to the interparticle contacts for medium and loose samples and
173 isotropically compressed the sample to p' = 50 kPa.

174 In this study, the relative density is defined at the isotropic mean normal stress used for the
175 micro-scale analysis (p' = 140 kPa). Samples were prepared by applying isotropic compression
176 through servomechanism by maximum strain rate of 1 s^{-1}. Samples with different friction
177 coefficients were isotropically compressed (p' = 140 kPa) similar to the densest state. A
178 comprehensive set of 25 samples (Table 2) with varying fine contents and gap ratios were
179 considered to cover internally stable, transitional zone and internally unstable gap graded soils
180 with non-plastic fine particles. In addition, Figure 2 shows particle size distribution curves for
181 samples with 10%≤FC≤50% and 2≤GR≤10.The number of particles was selected in order to

achieve an REV, which was checked using porosity, coordination number and the connectivity distribution.

Table 2 Number of Particles

FC	10 (%)		15 (%)		25 (%)		35 (%)		50 (%)	
GR	C	F	C	F	C	F	C	F	C	F
2	2512	3211	2512	5187	2512	9719	2512	15730	2512	29070
4	2512	26021	2512	41085	2512	77648	2512	125321	2512	232610
5	522	10542	522	16716	522	31618	522	50970	522	94692
7	522	28738	522	45703	522	86215	522	139238	522	259947
10	2512	404128	522	133062	522	251550	522	407504	522	757696

where, FC: Fine Content (%). GR: Gap Ratio, Number of Coarse Particles: C, Number of Fine Particles: F.

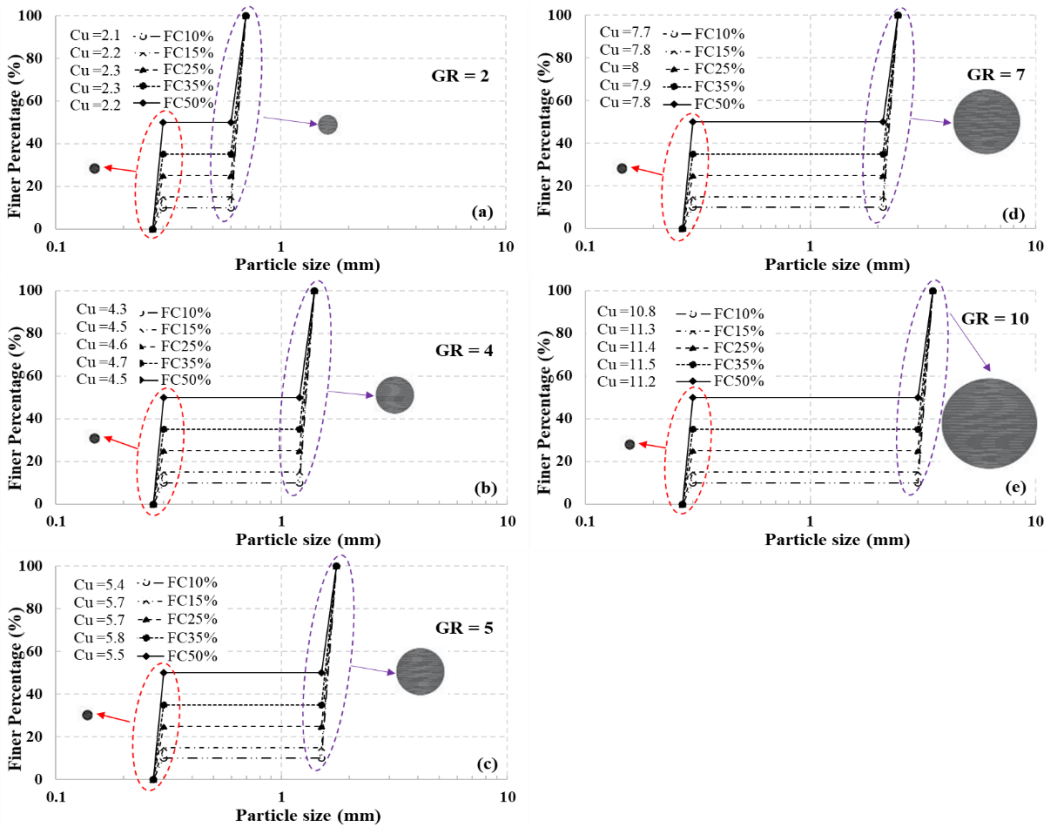

Figure 2. Particle Size Distribution Curves of the Simulated Soil Samples, (a) GR=2, (b) GR=4, (c) GR=5, (d) GR=7, (e) GR=10. Relative size of particles illustrated using circles.

Figure 3 presents the void ratio for samples with gap ratios of 2, 4 and 5 and 10% and 25% fine contents at p′ = 140kPa. Due to the minimal variation of void ratio when $\mu \geq 1$, e_{max} was quantified at μ=1. This study suggests considering friction coefficients of 0 and 1 to quantify e_{min} and e_{max} of granular non-plastic soils regardless of their real friction coefficient.

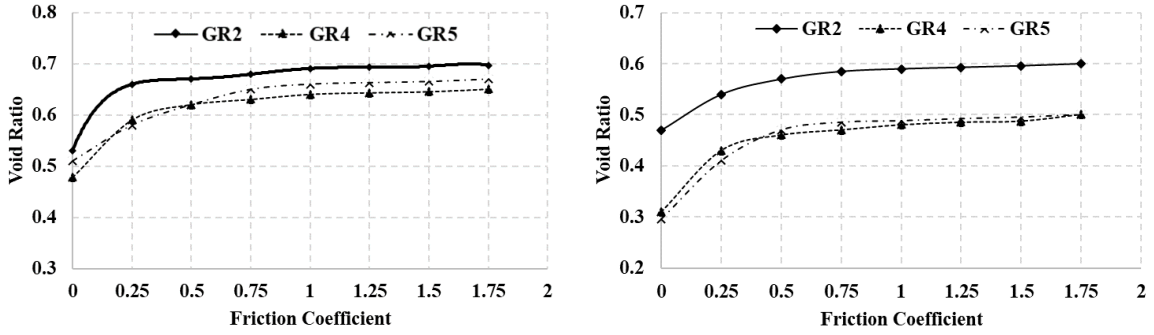

Figure 3. Variation of the sample void ratio with friction coefficient (a) sample with fine content of 10% and (b) sample with fine content of 25%

Absolute e_{min} (D_r=100%) and e_{max} (D_r=0%) are not often achievable under a specific experimental sample preparation method. Hence the minimum practical relative density ($D_{r,min}$) reported in experimental studies can be significantly higher than zero. In order to produce a sample with $D_{r,min}$ in DEM, μ was reduced from μ=1 (D_r=0%) to the friction coefficient of glass beads (μ_{soil}=0.3 [49]) under constant p' = 140 kPa (Figure 4). Figure 4 indicates that $D_{r,min}$ generally increases with an increase in the fine content until 30%≤FC≤35% and then decreases as fine content increases further. It is also evident that $D_{r,min}$ depends on gap ratio. For instance, $D_{r,min}$ does not vary noticeably by fine content when GR=2, as pore sizes are smaller than fine particles. Indeed, many researchers do not consider soils with GR = 2 to be truly gap-graded. Figure 5 shows that Z^{fine} (fine particles coordination number, Eq. 6 [13]) of packings at the $D_{r,min}$. Z^{fine} also increases with the gap ratio when 2≤GR≤7 and FC=35% and then decreases at GR=10. This is because the fine particles can form a continuous network and separate coarse particles more easily when GR=5 compared with GR=10.

$$Z^{fine} = \frac{\sum_{i=1}^{N_{p,fine}} (C_i^{fine-fine} + C_i^{fine-coarse})}{N_{p,fine}} \quad (6)$$

where $N_{p,fine}$= total number of fine particles; $C_i^{fine\text{-}fine}$= number of contacts between fine particle *i* and other fine particles; $C_i^{fine\text{-}coarse}$= number of contacts between fine particle *i* and other coarse particles.

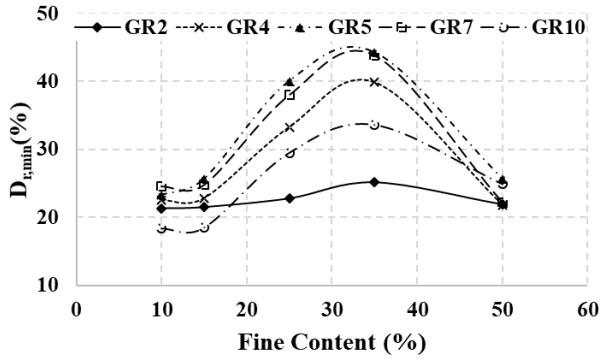

Figure 4. Variation of Dr,min with fine content and gap ratio

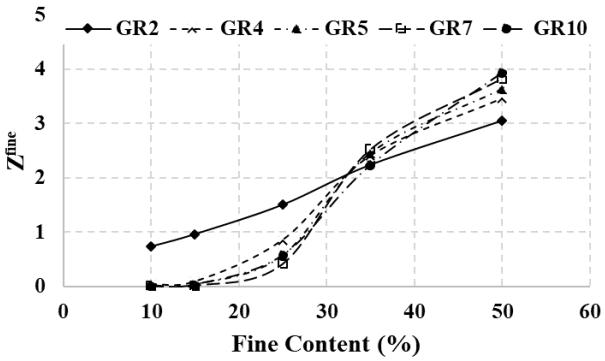

Figure 5. Variation of Z^{fine} at Dr,min with fine content and gap ratio

In order to reach higher relative densities, μ was gradually reduced by 0.01 from μ_{soil}=0.3 and then the sample was equilibrated at p' = 140 kPa. This procedure was repeated until the relative density degrees of 40, 50, 60, 70, 80, 90, and 100% (μ =0) were achieved (using Eq. 1). Before retrieving data, μ was reset to 0.3 to allow sample stresses to be properly compared. The proposed algorithm to produce the granular packing with different degrees of the relative density is exhibited in Figure 6.

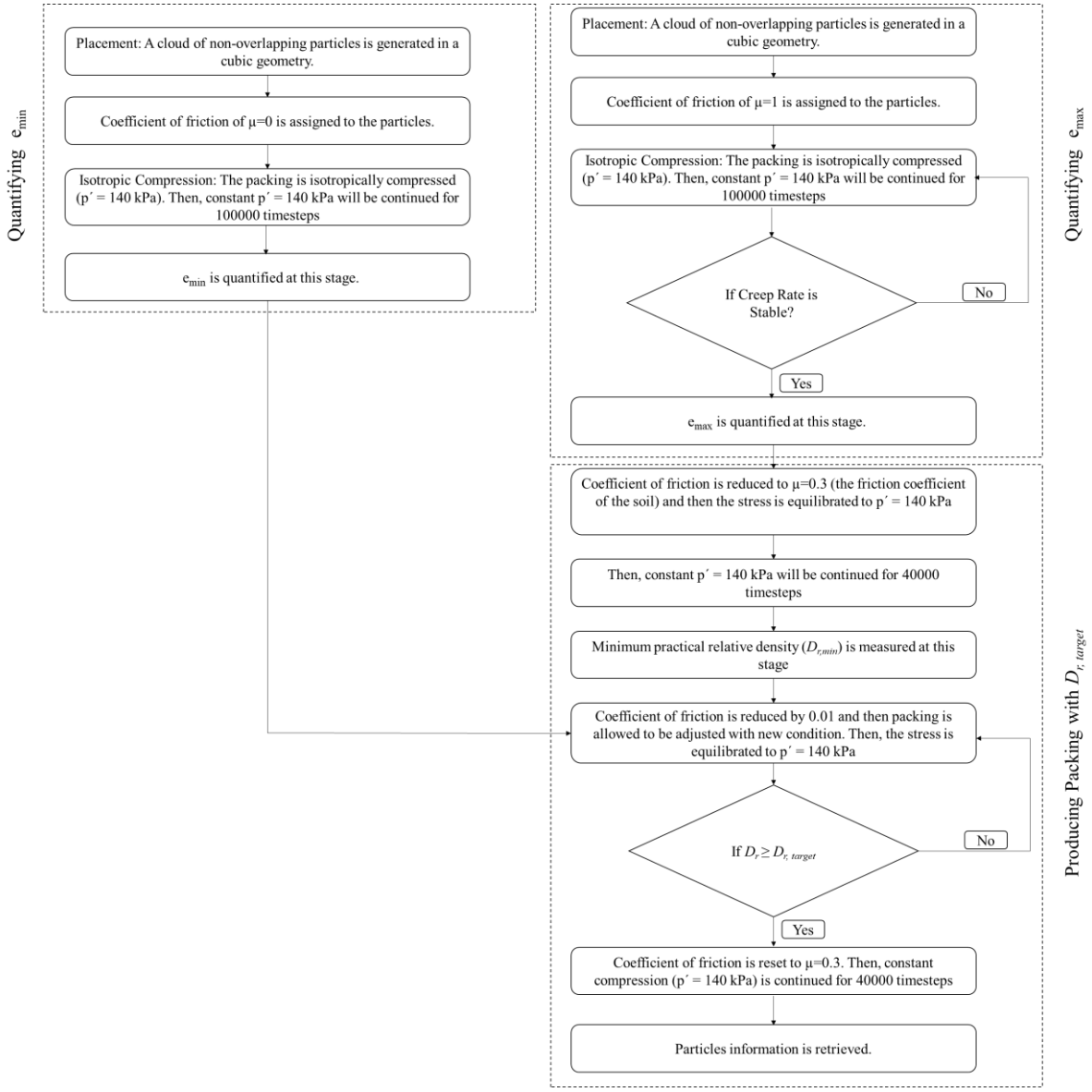

Figure 6. The developed algorithm for producing the granular packing with different degrees of the relative density

3. Results and Discussion

The relationship between relative density, α^{DEM} and different contact types is discussed in this section. Different contacts are formed in a gap graded soil sample including contacts between two fine particles (fine-fine), two coarse particles (coarse-coarse) and a fine particle and a coarse particle (coarse-fine).

3.1.Limiting void ratios

The variation of e_{min} and e_{max} for all samples are presented in Figure 7. Voids between the coarse particles are fully filled with the fine particles at the threshold fine content ($FC_{threshold}$, zone 2 in Figure 7). Hence, minimum value of e is achieved in zone 2 (25%≤FC≤35%) for all gap ratios.

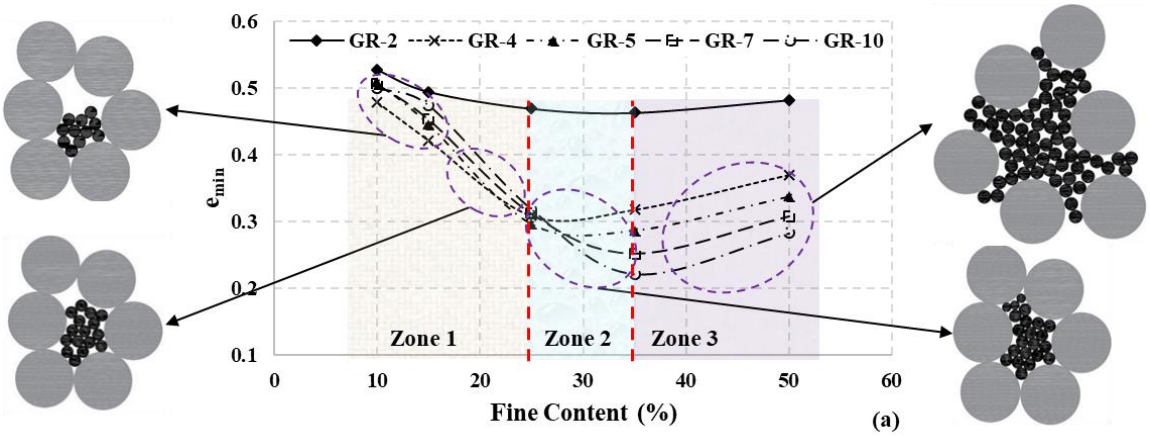

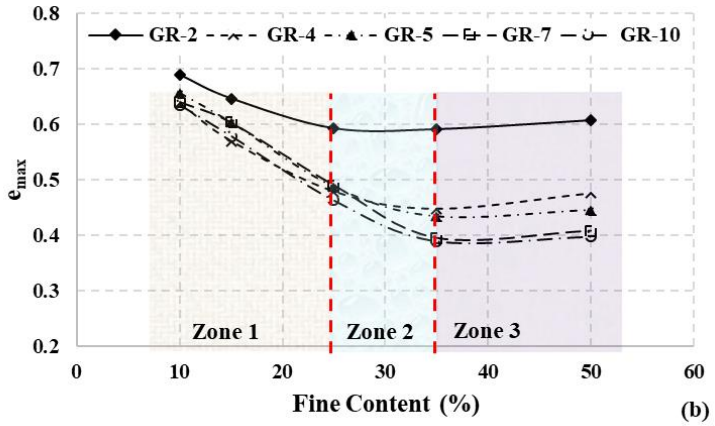

Figure 7. Variation of minimum (a) and maximum (b) void ratios with fine content and gap ratio

Comparisons with published experimental studies [50–53] show that there is a good agreement with experimental data on boundaries of zone 2 (25%≤FC≤35%). However, e_{min} and e_{max} values reported in this paper using DEM are not the same as experimental values reported in the literature due to the different standard methods used for the measurement of e_{min} and e_{max} and different particle shapes. Figure 7 indicates that the void ratio decreases as the fine content increases to the threshold value and then the void ratio increases with the fine content. Fine

particles fill the pre-existing voids between the coarse particles as the fine content increases before the threshold fine content, so the volume of voids decreases (zone 1 in Figure 7). Then, they will separate the coarse particles and increases the volume of the voids when $FC \geq FC_{threshold}$ (zone 3 in Figure 7). This pattern for the void ratio is confirmed by numerous experimental and numerical modelling studies [17,54–57]. The threshold fine content here varies from 25% to 35% for different samples (Figure 7) which is in agreement with previous studies [50–53,57–59].

3.2.Evaluation of homogeneity of samples

Sample homogeneity was checked by splitting the sample into layers and considering void ratio variation between each layer. Where particles overlapped layer boundaries, void ratio was calculated considering the proportion of particle volume in each layer. The distribution of void ratio and force network for some selected samples are presented in Figures 8-9.

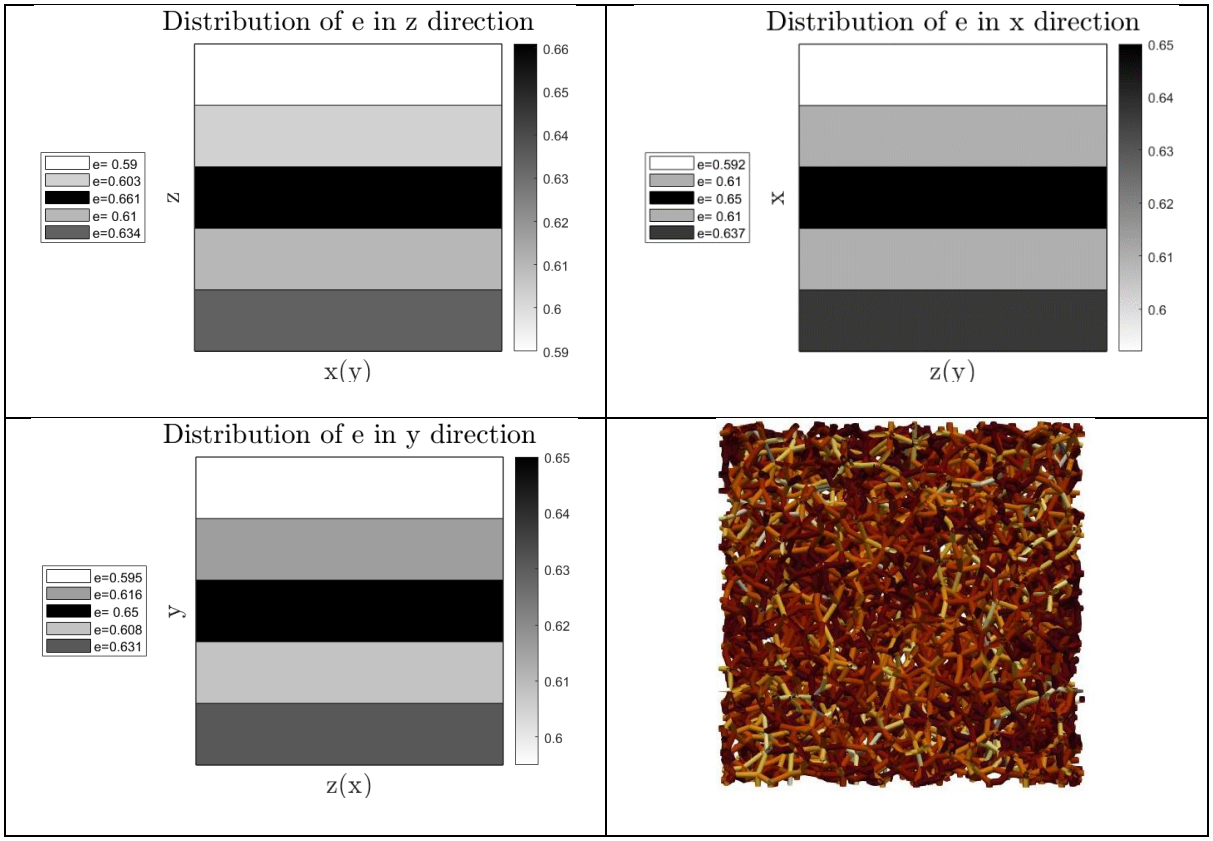

Figure 8. Distribution of Void Ratio and Contact Force Network for Sample with Gr=2, FC=35% (Loosest State)

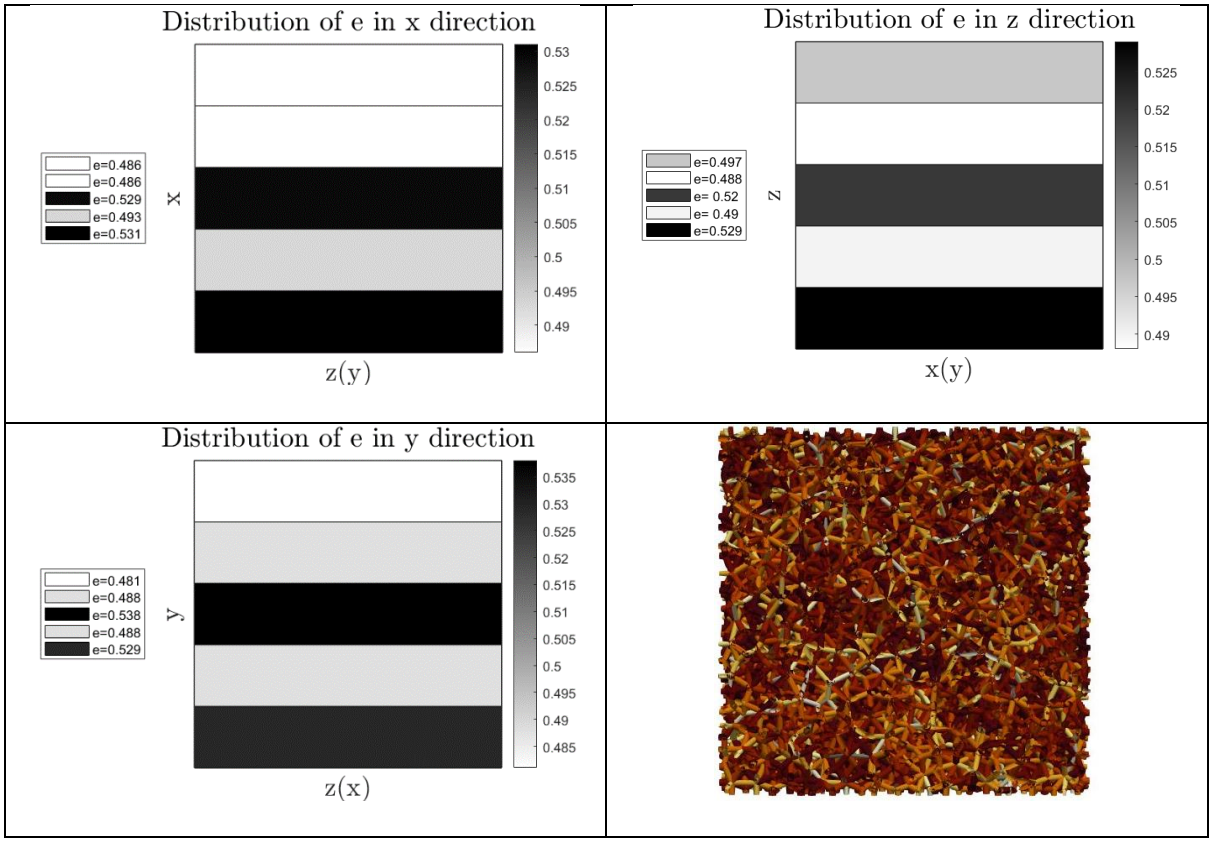

Figure 9. Distribution of Void Ratio and Contact Force Network for Sample with Gr=2, FC=35% (Dr=100%)

3.3. The influence of relative density on α^{DEM}

Figure 10 (a and b) demonstrate the variation of α^{DEM} with relative density and gap ratio when FC≤15%. Two behaviour types are presented in Figure 10: Type 1(α^{DEM} increases with relative density) and Type 2 (α^{DEM} does not change with relative density). Behaviour Type 1 is observed when GR=2 and FC≤15% in Figure 10 (a and b). This behaviour was expected for the sample with GR=2 because the size of the fine particles is larger than the pore size and the majority of the fine particles are actively participating in the force network even when FC=10%. However, when the gap ratio is higher (4≤GR≤10), the size of fine particles is not large enough to fill pores between coarse particles. Hence, the coarse fraction forms a continuous contact network and the relative density has minimal influence on α^{DEM} (behaviour Type 2). The α^{DEM} slightly decreases as the relative density increases when GR≥5. This pattern shows that strength of

contact between the coarse particles improves with a relative density which is in good agreement with numerical results presented by Shire et al. [13].

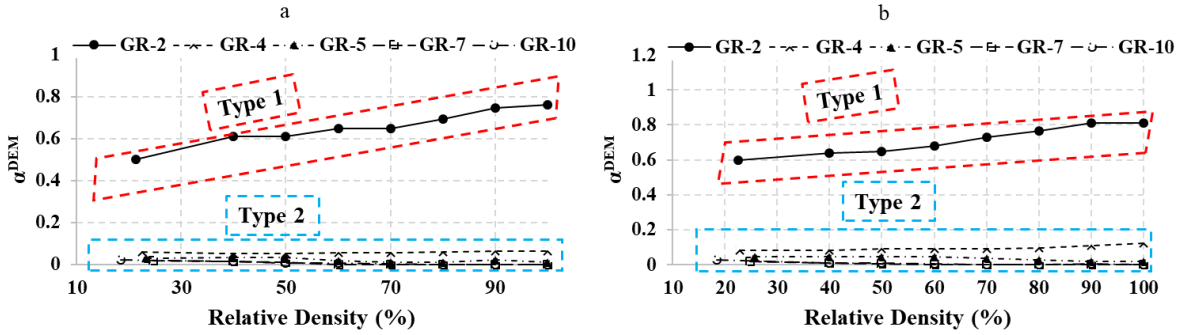

Figure 10. Variation of average α^{DEM} with gap ratio and relative density when (a) FC=10% and (b) FC=15%

The influence of the relative density on α^{DEM} when FC=10% is also demonstrated in Table 3. The first column demonstrates the initial state of the sample in Table 3-5 ($\alpha^{DEM}\geq 0$). However, particles which are not transferring stress ($\alpha^{DEM}=0$) are removed from the images in other columns to visually investigate the effects of relative density on fine particles contribution to the load-carrying mechanism. Table 3 indicates that the majority of fine fraction carries zero stress when GR≥4 and FC≤15% regardless of relative density. On the contrary, as relative density increases, the slight increase in the number of fine particles with $\alpha^{DEM}>0$ can be observed when GR=2.

Table 3. Images of packings with FC=10%

Initial Sample State	GR				
	2	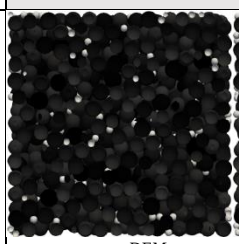			Behaviour Type 1
$\alpha^{DEM}\geq 0$		D_r=40%, α^{DEM}=0.61	D_r=70%, α^{DEM}=0.65	D_r=100%, α^{DEM}=0.76	
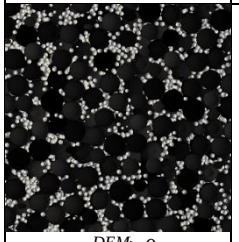	4	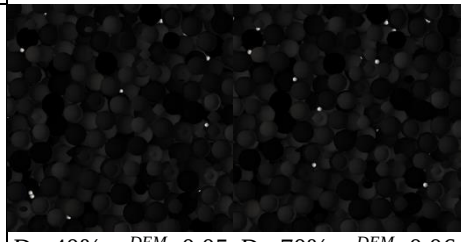		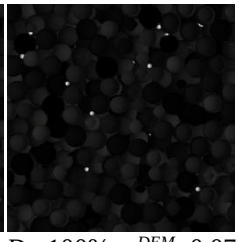	Behaviour Type 2
$\alpha^{DEM}\geq 0$		D_r=40%, α^{DEM}=0.05	D_r=70%, α^{DEM}=0.06	D_r=100%, α^{DEM}=0.07	

Figure 11 illustrates the variation of α^{DEM} with relative density and gap ratio when 25%≤FC≤35%. Behaviour Type 3 (soil is internally stable, α^{DEM}>0.8 even at $D_{r,min}$) is observed for samples with GR=2 and FC=25% and 35%. Behaviour Type 2 was again observed for the packings with GR≥5 and FC=25%. Figure 11 (a) indicates that the sensitivity of the sample with GR=4 to relative density starts form FC=25% and α^{DEM} increases gradually when D_r≥50 (behaviour Type 1). However, α^{DEM} increases continuously with relative density when GR≥4 and FC=35% (Figure 11 (b)). Figure 7 shows that the threshold fine content for e_{min} and e_{max} curves when GR=4 is 25% and 32%, respectively, while the threshold fine content is higher when GR≥5. Making a comparison between the threshold fine content of the samples with various gap ratios reveals that pre-existing pores between coarse particles are filled with fine particles in a lower fine fraction when GR=4 than GR≥5. Hence, the contribution of fine particles to the load-carrying mechanism and in other words sensitivity to relative density starts at a lower fine content when GR=4. The number of fine particles with α^{DEM}>0 increases as relative density increases when 2≤GR≤4 and FC=25%. However, the marginal contribution of the fine particles to the soil matrix can be observed when GR≥5 and FC=25%.

Table 4 indicates that when GR=5 and FC=25% the majority of the fine particles are under-stressed and can be washed out by seepage flows.

Figure 11 (b) shows the behaviour Type 1 for samples with GR≥4 and FC=35%. According to Kezdi's criterion [60], the soils samples with GR=4 and 5 are located close to the geometric borderline of internal instability but they become stable according to the stress criterion (α^{DEM}≥0.8) at 65% and 75% relative density, respectively, when FC=35%. This trend was also confirmed by Indraratna et al.[23]. Samples with GR=7 and 10 become internally stable at D_r=80% and 90%, respectively.

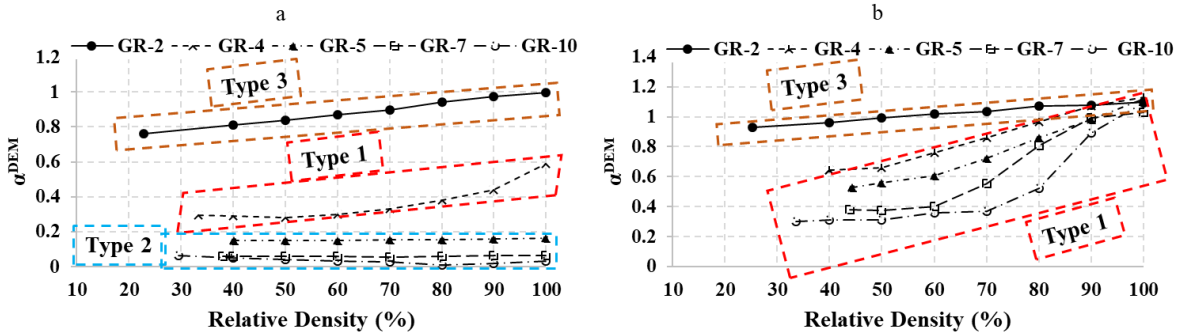

Figure 11. Variation of average α^{DEM} with gap ratio and relative density when (a) FC=25% and (b) FC=35%

Table 4. Images of packings with FC=25%

Initial Sample State	GR				
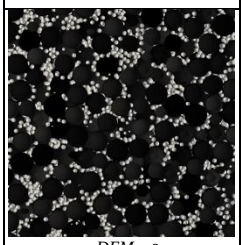	2		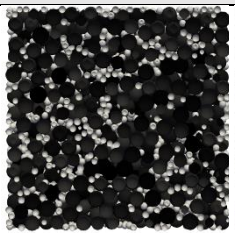	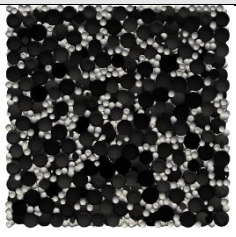	Behaviour Type 3
$\alpha^{DEM}\geq 0$		D_r=40%, α^{DEM}=0.81	D_r=70%, α^{DEM}=0.9	D_r=100%, α^{DEM}=1	
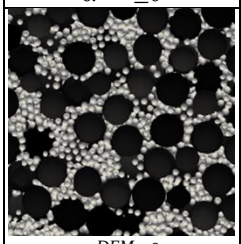	4	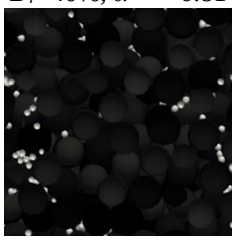	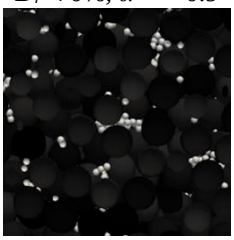	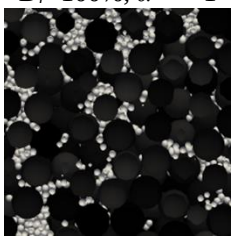	Behaviour Type 1
$\alpha^{DEM}\geq 0$		D_r=40%, α^{DEM}=0.29	D_r=70%, α^{DEM}=0.33	D_r=100%, α^{DEM}=0.59	
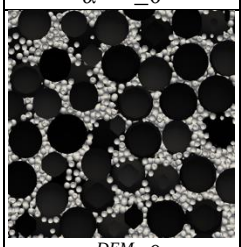	5	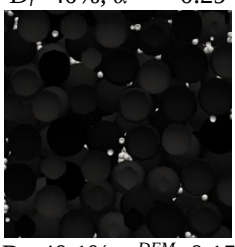	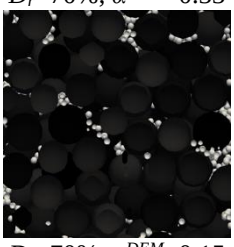	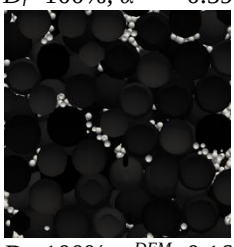	Behaviour Type 2
$\alpha^{DEM}\geq 0$		D_r=40.1%, α^{DEM}=0.15	D_r=70%, α^{DEM}=0.15	D_r=100%, α^{DEM}=0.16	

Table 5 displays images of samples with FC=35% and 2≤GR≤10. Apart from the sample with GR=2 which is stable even at $D_{r\,min}$, the sensitivity of samples with GR≥4, can be observed as the number of fine particles with α^{DEM}>0 increases with relative density in Table 5.

Figure 12 presents the behaviour Type 3 for samples with GR≥2 and FC=50%. It can be seen that α^{DEM} is not sensitive to gap ratio but increases slightly with relative density. In all cases $\alpha^{DEM}\geq 1$ and it can be concluded these samples are internally stable.

Table 5. Images of packings with FC=35%

Initial Sample State	GR				
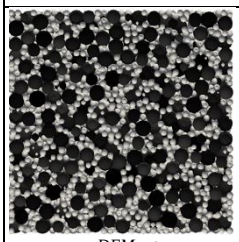	2	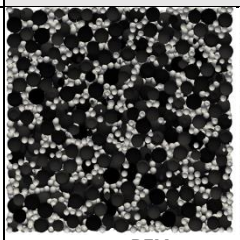	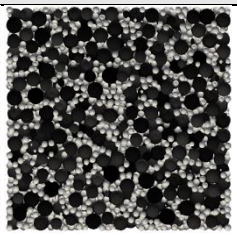	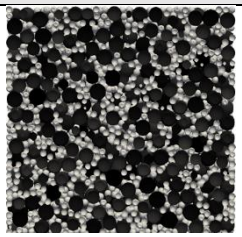	Behaviour Type 3
$\alpha^{DEM}\geq 0$		D_r=40%, α^{DEM}=0.96	D_r=70%, α^{DEM}=1.03	D_r=100%, α^{DEM}=1.1	
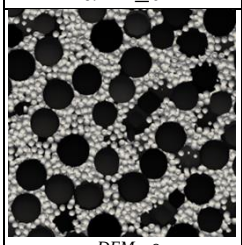	4	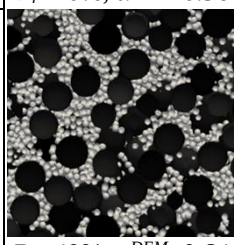	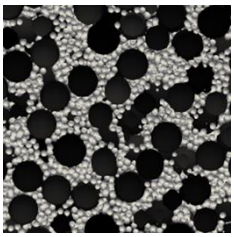	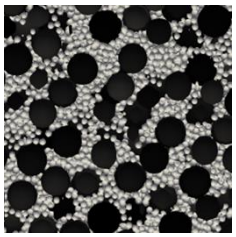	Behaviour Type 1
$\alpha^{DEM}\geq 0$		D_r=40%, α^{DEM}=0.64	D_r=70%, α^{DEM}=0.86	D_r=100%, α^{DEM}=1.13	
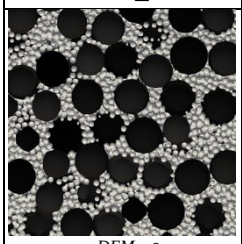	5	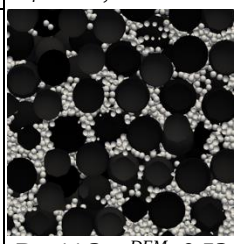	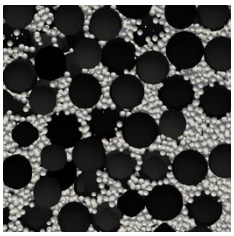	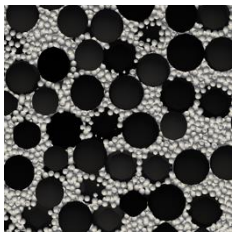	Behaviour Type 1
$\alpha^{DEM}\geq 0$		D_r=44.3, α^{DEM}=0.53	D_r=70%, α^{DEM}=0.72	D_r=100%, α^{DEM}=1.12	
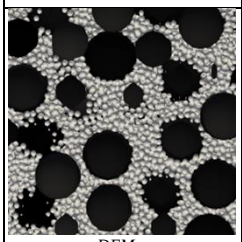	7	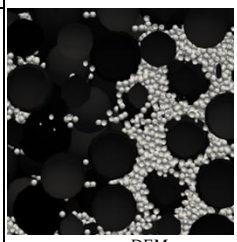	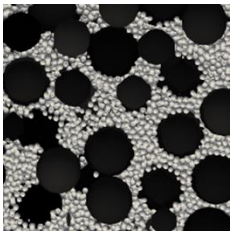	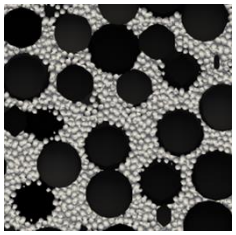	Behaviour Type 1
$\alpha^{DEM}\geq 0$		D_r=43.8, α^{DEM}=0.38	D_r=70%, α^{DEM}=0.55	D_r=100%, α^{DEM}=1.03	
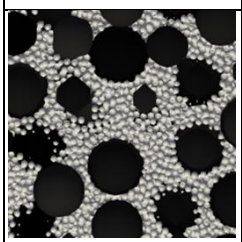	10	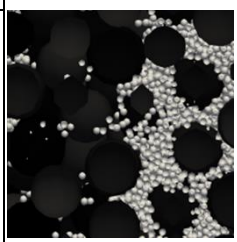	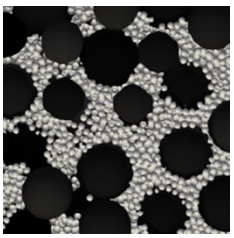	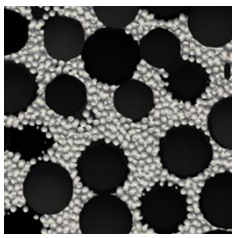	Behaviour Type 1
$\alpha^{DEM}\geq 0$		D_r=40%, α^{DEM}=0.31	D_r=70%, α^{DEM}=0.37	D_r=100%, α^{DEM}=1.09	

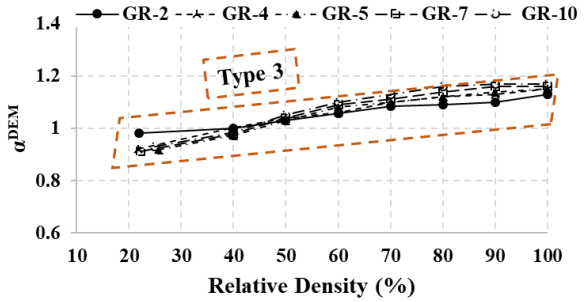

Figure 12. Variation of average α^{DEM} with gap ratio and relative density when FC=50%

Figure 13 summarize the variation of α^{DEM} with respect to the fine content, gap ratio and the relative density. Figure 13b presents three cross sections of Figure 13a to show the influence of relative density on α^{DEM} more clearly. It can be seen that α^{DEM} is quite high when FC≥10%, GR<4 (internally stable) and D_r≥40%. In such cases α^{DEM} increases as D_r increases. Moreover, α^{DEM} doesn't change noticeably with the relative density when 10%≤FC≤25% and GR>5 (internally unstable), while α^{DEM} increases with relative density when FC>25% and GR>5. A gap graded soil is overfilled when FC≥35% and the coarse particles float in the fine particle matrix. Therefore, the gap ratio doesn't play an important role in the contribution of the fine particles to the load-carrying mechanism. The variation of α^{DEM} when 4≤GR≤5 with the fine content and the relative density can be seen in Figure 13. The soil is underfilled and internally unstable when FC<25% and 4≤GR≤5. The soil is overfilled and internally stable when FC>35% and 4≤GR≤5. However, the soil fits within the transitional zone as relative density increases when 25%≤FC≤35% and 4≤GR≤5.

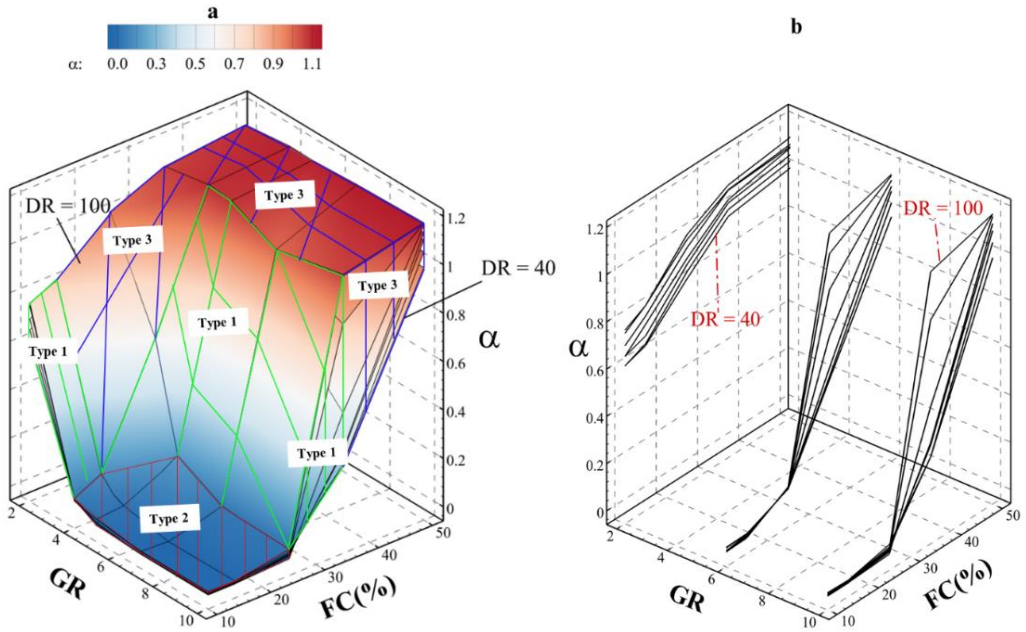

Figure 13. Variation of average α^{DEM} with gap ratio, fine content and relative density

Table 6 summarises the influence of relative density on internal stability of gap graded samples with 2≤GR≤10 and 10%≤FC≤50%.

Table 6 Influence of relative density on internal stability state of gap graded soils

GR	FC (%)	D_r (%)				GR	FC (%)	D_r (%)			
		Min	60	80	100			Min	60	80	100
2	10	GS[1]	GS	GS	GS	7	10	U	U	U	U
	15	GS	GS	GS	GS		15	U	U	U	U
	25	S[2]	S	S	S		25	U	U	U	U
	35	S	S	S	S		35	B	B	S	S
	50	S	S	S	S		50	S	S	S	S
4	10	U[3]	U	U	U	10	10	U	U	U	U
	15	U	U	U	U		15	U	U	U	U
	25	U	U	B	B		25	U	U	U	U
	35	B[4]	B	S	S		35	U	U	B	S
	50	S	S	S	S		50	S	S	S	S
5	10	U	U	U	U						
	15	U	U	U	U						
	25	U	U	U	U						
	35	B	B	S	S						
	50	S	S	S	S						

1- GS: $0.4 \leq \alpha^{DEM} \leq 0.8$, but geometric susceptibility criterion is not met. Hence, fine particles cannot be eroded and the soil is internally stable
2- S: Sample is stable and $\alpha^{DEM} > 0.8$
3- U: Sample is unstable; $\alpha^{DEM} < 0.4$
4- B: Sample is on the borderline of internal stability and suffusion initiates under the existence of large enough seepage forces; $0.4 \leq \alpha^{DEM} \leq 0.8$

3.4.The influence of relative density on contact types

Coarse-coarse (*C*-*C*), fine-coarse (*F*-*C*) and fine-fine (*F*-*F*) contacts can form in a granular packing [35]. The percentage of each contact type are calculated through Eqs. 7-9.

$$C - C\ (\%) = \frac{N_{c,coarse-coarse}}{N_c} \times 100 \qquad (7)$$

where N_c= number of contacts in the packing and $N_{c,coarse-coarse}$= number of coarse-coarse particle contacts..

$$F - C\ (\%) = \frac{N_{c,fine-coarse}}{N_c} \times 100 \qquad (8)$$

where $N_{c,fine-coarse}$= number of contacts between fine and coarse particles.

$$F - F\ (\%) = \frac{N_{c,fine-fine}}{N_c} \times 100 \qquad (9)$$

where $N_{c,fine-fine}$= number of fine-fine particle contacts.

Contact types are considered as strong when the contact force is greater than average contact force [35]. Eqs. 10-12 are used for calculation of the percentage of each strong contact type.

$$Strong_{C-C}\ (\%) = \frac{N_{c,strong_{coarse-coarse}}}{N_{c,strong}} \times 100 \qquad (10)$$

where $N_{c,strong_{coarse-coarse}}$ = number of coarse-coarse contacts with contact force≥average contact force; $N_{c,strong}$ = number of strong contacts in the packing.

$$Strong_{f-C}\ (\%) = \frac{N_{c,strong_{fine-coarse}}}{N_{c,strong}} \times 100 \qquad (11)$$

where $N_{c,strong_{fine-coarse}}$ = number of fine-coarse contacts with contact force≥average contact force.

$$Strong_{f-f}\ (\%) = \frac{N_{c,strong_{fine-fine}}}{N_{c,strong}} \times 100 \qquad (12)$$

where $N_{c,strong_{fine-fine}}$ = number of fine-fine contacts with contact force≥average contact force.

Figure 14 shows the variation of contact type and strong contact type percentage with relative density when GR=4 and FC=25%. The number of coarse-coarse contacts inside the sample increase until D_r=50% and then decreases with relative density (Figure 14 (a)). The number of fine-coarse contacts is relatively constant with relative density. However, the number of fine-fine contacts decreases as relative density increases until D_r=50% and then increases with the relative density. The sensitivity of the fine fraction's contribution to the soil fabric to the relative density can be observed in variation of contact types with relative density at GR=4 and FC=25%. Figure 14 (b) shows a similar but more pronounced trend for strong contact types.

Figure 15 displays a variation of contact type and strong contact type percentages with relative density when GR=4 and FC=35%. It can be clearly observed that the coarse-coarse contacts' role is negligible. Packing behaviour is governed by fine-coarse contacts according to Figure 15 (b) when $D_r \leq 50\%$. Then, fine-fine contacts overcome other contact types and form a continuous strong contact network.

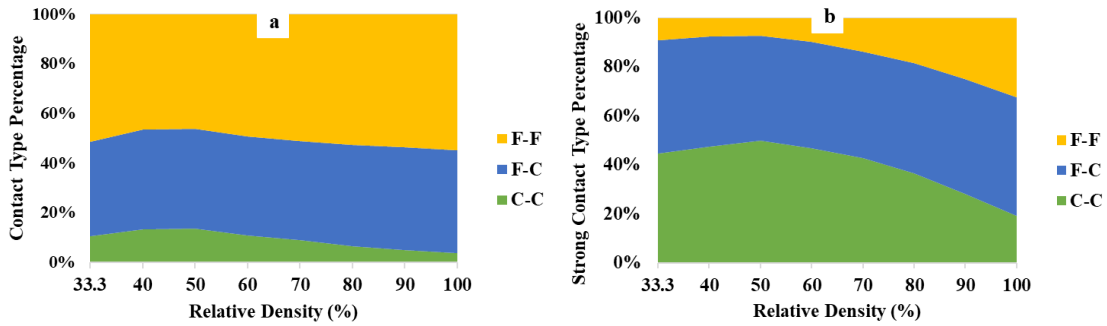

Figure 14. Variation of (a) contact type and (b) strong contact type percentage with relative density when GR=4 and FC=25%

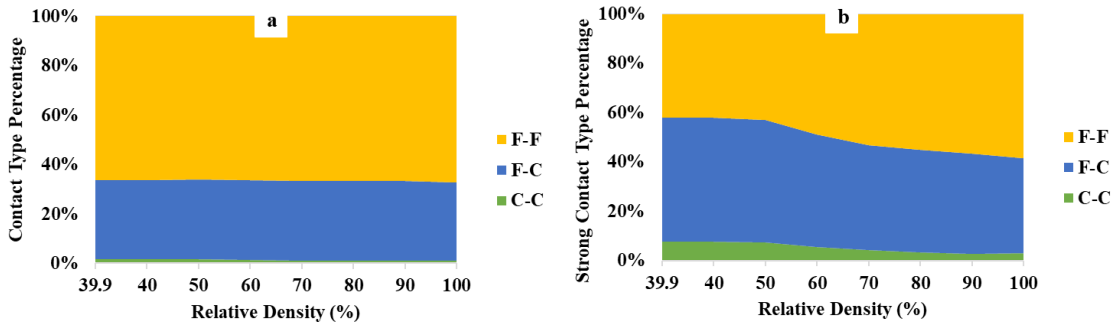

388

389 *Figure 15. Variation of (a) contact type and (b) strong contact type percentage with relative density when GR=4*
390 *and FC=35%*

391

392 The transitional behaviour of gap graded granular packings can be attributed to the role that
393 strong fine-coarse contacts play when GR=4 and 25≤FC≤35 (Figure 14 and 15). Strong fine-
394 coarse contacts dominate the packing's behaviour when FC=25% and this trend continues as
395 fine content increases to 35% and D_r=50%. Then, strong fine-fine contacts govern the soil
396 behaviour when D_r>50%.

397 Figure 16 shows the relationship between α^{DEM} and Z^{fine} when GR≥4. Similar to α^{DEM}, Z^{fine}
398 values are low and the relative density has no effect on Z^{fine} when the behaviour of the material
399 follows Type 2. In Type 1, Z^{fine} increases with α^{DEM} as the relative density increases. The
400 material behaves similar to Type 2 at low relative densities and then, it approaches Type 3 by
401 passing through transitional zone. Z^{fine} varies between 0-1.25, 1.6-4.2 and 4-5.6 for the
402 underfilled, transitional zone and overfilled sample, respectively. Z^{fine}≥4 can be considered as
403 a stable range for the fine fraction. Hence, Z^{fine} can be a good representative of stability of the
404 sample as it is quite low in underfilled samples, increases with relative density in the
405 transitional zone and it is greater than 4 when soil is overfilled.

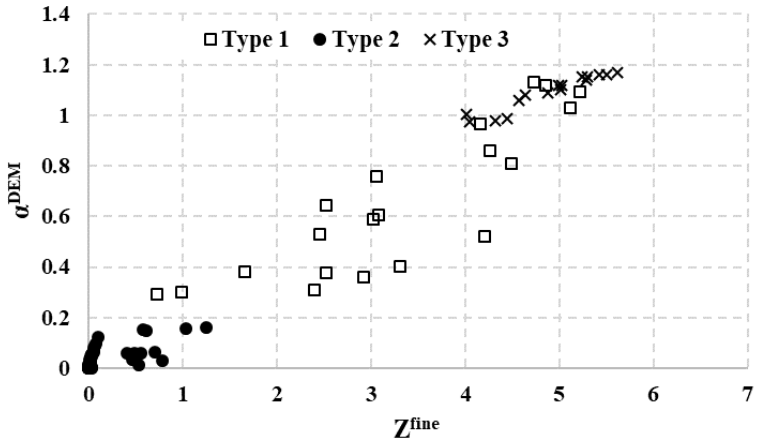

406

407 *Figure 16. Variation of α^{DEM} with Z^{fine}*

408

409 Crawford-Flett [61] developed intergranular matrix phase diagrams in fine content-void ratio
410 space for different gap graded materials. Gap graded soil intergranular matrix is divided into
411 three types: Type C: Coarse fraction governs the soil behaviour; Type M: Fine fraction
412 dominates the behaviour; Type T: A transition from Type C to Type M occurs in which both
413 fine and coarse fractions contribute to the soil fabric [61].

414 Thevanayagam and Mohan [32] proposed intergranular matrix phase diagrams with different
415 zones for gap graded soil (a mixture of sand and silt). Figure 17 (a, b, c and d) show the
416 intergranular matrix phase diagrams of gap graded granular assemblies with gap ratio of 4, 5,
417 7 and 10, respectively. In terms of stress transfer and connectivity characteristics, soils with
418 GR≤2 are similar to uniform soils [17], so a soil with GR=2 is not presented. The impact of
419 increasing the relative density on α^{DEM} is depicted using a coloured square ($\alpha^{DEM}<0.4$), triangle
420 ($0.4\leq\alpha^{DEM}\leq0.8$) and circle ($\alpha^{DEM}>0.8$). Coloured zones representing different cases based on
421 Thevanayagam and Mohan [32] can show the influence of relative density on change of soil
422 case for varying fine content and gap ratio.

423 According to Thevanayagam and Mohan [32], the intergranular matrix state of gap graded soil
424 can be categorized into four cases. Cases 1 to 3 occur when $FC\leq FC_{threshold.}$ In Case 1, e_c (Eq.

13, void ratio of the pure coarse fraction) $<e_{c,max}$ (maximum void ratio of the pure coarse fraction) and e_f (Eq. 14, void ratio of the pure fine fraction) is very high and coarse particles form a continuous network controlling the soil behaviour.

$$e_c = \frac{e+FC/100}{1-FC/100} \quad (13)$$

$$e_f = \frac{e}{FC/100} \quad (14)$$

In Case 2, $e_c \approx e_{c,max}$ and the fine particles fit inside the pores between coarse particles (i.e. the soil is underfilled). In Case 3, relative density is low (high void ratio, $e_c > e_{c,max}$), most of the coarse particles are separated by fine particles. However, due to the low relative density and fine content ($FC \leq FC_{threshold}$), fine particles do not form a continuous contact network (underfilled). Hence, the fine fraction can be eroded (internally unstable) if large enough hydraulic gradient is applied to the soil when soil is classified as Cases 1-3. Case 4 happens when $FC > FC_{threshold}$ (e_f is very low) and the fine content is sufficiently high to form a continuous contact network (overfilled, or internally stable). As $FC_{threshold}$ is dependent of gap ratio and relative density, there is a transitional zone from Case 3 to 4.

It can be seen in Figure 17 that scattered data are fitted well between $e_{c,max}$ and $e_{c,min}$ when $10\% \leq FC \leq 15\%$ and $4 \leq GR \leq 10$. This shows that the intergranular matrix state is fitted within the range of Case 2 at low relative densities but Case 1 is observed at high relative densities until FC=15%. These packings are also classified as underfilled based on α^{DEM}.

Figure 17 shows that the packings' intergranular matrix state locates in Case 3 at low relative densities and then, they enter Case 2 region as relative density increases when FC=25% and $4 \leq GR \leq 10$. The gap graded packings intergranular matrix fit within the transition from Case 3 to Case 4 region for packings with FC=35% and $4 \leq GR \leq 10$. Indeed, the intergranular matrix properties of the soil is similar to Case 3 (internally unstable) when relative density is low but

samples become internally stable (Case 4) as relative density increases. α^{DEM} also shows the same pattern for these packings. Case 4 can be observed in Figure 17 when FC=50% regardless of relative density and gap ratio.

Correlation of Cases 1-4 expressing the intergranular matrix state of the soil at macro-level, with defined ranges for α^{DEM} which is micro-scale properties of the packing in Figure 17 shows that α^{DEM} is a good representative of intergranular matrix state of the packing.

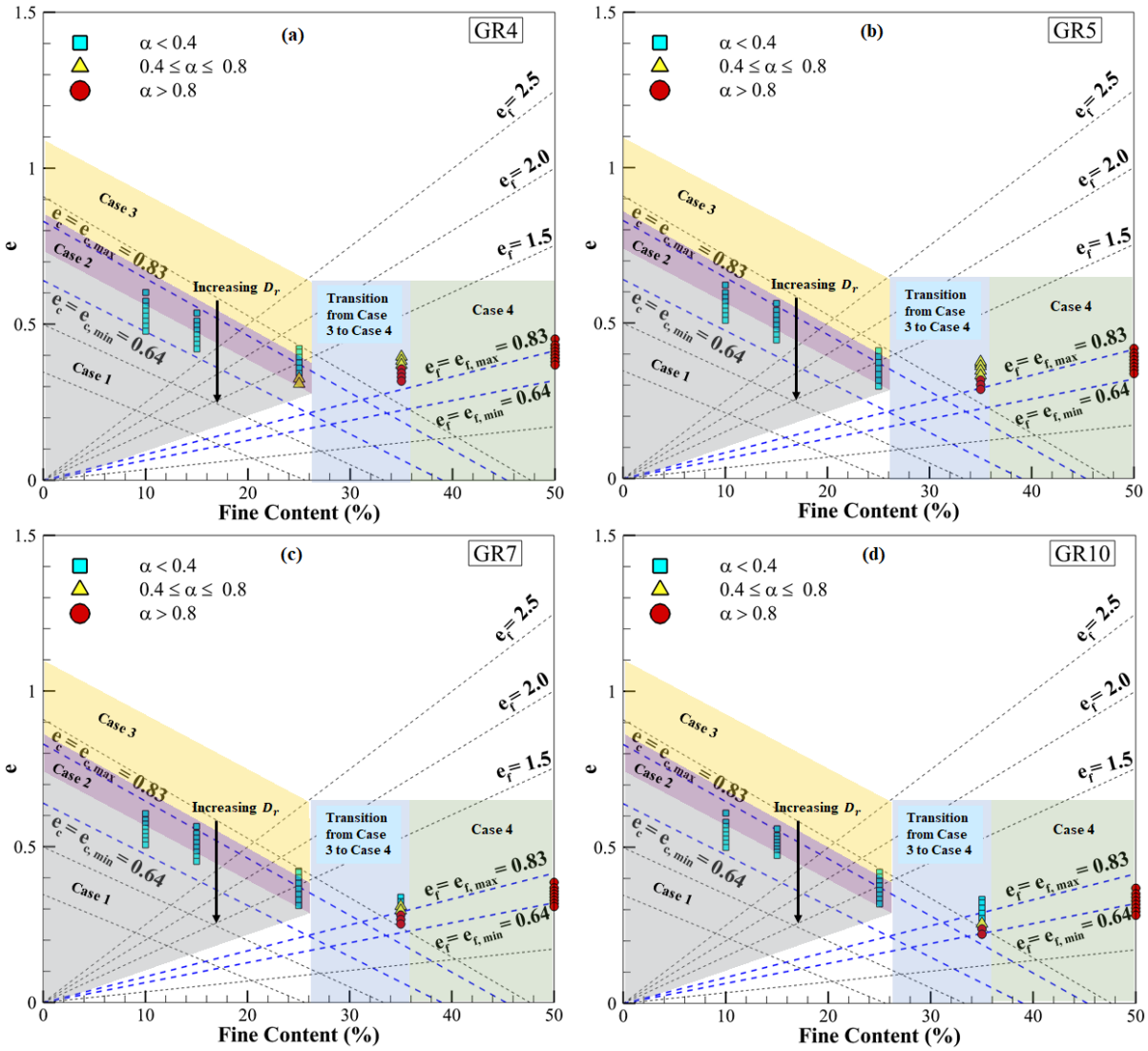

Figure 17. Intergranular matrix phase diagrams (a) GR=4, (b) GR=5, (c) GR=7, (d) GR=10

4. Conclusions

This paper proposed a procedure to produce a granular packing with different degrees of relative densities in DEM. The influence of the relative density on internal stability of gap graded packings with a wide range of gap ratios and fine contents was investigated. The relative density of each packing was increased from minimum value to 100% and α^{DEM}, contact types and strong contact types percentages were investigated for each packing. It was understood that α^{DEM} was sensitive to relative density when GR=2 and FC≤25%. Although the fine content was low, the contribution of the fine fraction to the soil matrix increased with an increase in the relative density. Using perfectly spherical particles with free particle rotation allowed large numbers of gap-graded particles to be modelled, but can be indicated as a limitation of the current study. Following are concluding remarks which can be drawn from the current study:

(a) A soil with GR≥4 and FC≤15% remains internally unstable regardless of the degree of relative density as coarse fraction forms a continuous contact network and the majority of fine particles are under-stressed inside the voids between coarse particles. This trend is in agreement with previous studies and internal stability criteria.

(b) The sensitivity of soil with GR=4 to the relative density starts from FC=25% because voids between coarse particles are filled with fine particles ($FC \approx FC_{threshold}$). The soil is internally unstable until D_r=80%. However, the soil enters the transitional zone when $80\% \leq D_r \leq 100\%$.

(c) Samples with FC=35% and 4≤GR≤7 are in the transitional zone at low relative densities and become internally stable by an increase in the relative density. When GR=10 and FC=35%, the packing is internally unstable at low relative densities, then it enters the transitional zone and finally becomes internally stable as relative density increases. Relative density can affect the internal stability of the soil when soil is close to the

485 borderline of internal stability. This trend is in a good agreement with experimental
486 findings of Indraratna et al. [23].
487 (d) α^{DEM} remains relatively constant ($\alpha^{DEM}\approx1$) when FC=50% regardless of relative density
488 and gap ratio. Indeed, the soil is internally stable and fine fraction forms a continuous
489 network which governs the soil behaviour.
490 (e) Similar to α^{DEM} which determines the internal stability status of the gap graded granular
491 packing, Z^{fine} also is a reliable microscopic parameter which relates connectivity data
492 to the internal stability of the sample.
493 (f) Fine-coarse contacts dominate the gap graded packings behaviour in the transitional
494 zone. The percentage of strong fine-coarse contacts remains relatively constant with
495 relative density, but the percentage of strong fine-fine contacts increases as relative
496 density increases. The transition from being governed by fine-coarse to fine-fine
497 contacts confirms that stability of fine fraction matrix improves with relative density.
498 (g) There is a good agreement between micro-scale findings (α^{DEM} and its relationship with
499 internal stability status of the sample) and macro-scale matrix phase diagrams which
500 confirms the validity of micro-scale information.

501 **Acknowledgements:**

502 The authors would like to thank Dr Mahyar Madadi from the University of Melbourne for
503 sharing his mathematical and analytical experience in granular material. We would like to
504 acknowledge Mr Kenichi Kawano from Kajima Corporation, Tokyo, Japan for providing his
505 experience of PFC software. The first author is the recipient of the Melbourne Research
506 Scholarship from The University of Melbourne.

507

508

Data Statement:

All data, models, or code generated or used during the study are available from the corresponding author by request.

References

[1] Foster M, Fell R, Spannagle M. The statistics of embankment dam failures and accidents. Can Geotech J 2000;37:1000–24. https://doi.org/10.1139/t00-030.

[2] US Department of the Interior Bureau of Reclamation. Internal Erosion Risks for Embankments and Foundations. Best Pract Dam Levee Saf Risk Anal 2015:1–134.

[3] Yang J, Yin ZY, Laouafa F, Hicher PY. Analysis of suffusion in cohesionless soils with randomly distributed porosity and fines content. Comput Geotech 2019;111:157–71. https://doi.org/10.1016/j.compgeo.2019.03.011.

[4] Mehdizadeh A, Disfani MM, Evans R, Arulrajah A, Ong DEL. Mechanical consequences of suffusion on undrained behaviour of a gap-graded cohesionless soil-an experimental approach. Geotech Test J 2017;40:1026–42. https://doi.org/10.1520/GTJ20160145.

[5] Yang J, Yin Z-Y, Laouafa F, Hicher P-Y. Hydro-mechanical modeling of granular soils considering internal erosion. Can Geotech J 2019:1–53. https://doi.org/10.1139/cgj-2018-0653.

[6] Bonelli S, Marot D. On the modelling of internal soil erosion. 12th Int Conf Comput Methods Adv Geomech 2008 2008;4:2544–50.

[7] Fell R, Wan CF, Cyganiewicz J, Foster M. Time for Development of Internal Erosion and Piping in Embankment Dams. J Geotech Geoenvironmental Eng 2003;129:307–14. https://doi.org/10.1061/(ASCE)1090-0241(2003)129:4(307).

[8] Kawano K, Shire T, O'Sullivan C. Coupled particle-fluid simulations of the initiation of suffusion. Soils Found 2018;58:972–85. https://doi.org/10.1016/j.sandf.2018.05.008.

[9] Fannin J, Slangen P, Ataii S, McClelland V, Hartford D. Erosion of zoned earthfill dams by internal instability: laboratory testing for model development. Eur. Work. Gr. Intern. Eros., Springer; 2018, p. 34–49.

[10] Rochim A, Marot D, Sibille L, Le VT. Effects of hydraulic loading history on suffusion susceptibility of cohesionless soils. J Geotech Geoenvironmental Eng 2017;143:1–10. https://doi.org/10.1061/(ASCE)GT.1943-5606.0001673.

[11] Sterpi D. Effects of the erosion and transport of fine particles due to seepage flow. Int J Geomech 2003;3:111–22. https://doi.org/10.1061/(ASCE)1532-3641(2003)3:1(111).

[12] Garner SJ, Fannin RJ. Understanding internal erosion: a decade of research following a sinkhole event. Int J Hydropower Dams 2010;17:93–8.

[13] Shire T, O'Sullivan C, Hanley KJ, Fannin RJ. Fabric and effective stress distribution in internally unstable soils. J Geotech Geoenvironmental Eng 2014;140:1–11. https://doi.org/10.1061/(ASCE)GT.1943-5606.0001184.

[14] Shire T, O'Sullivan C. Constriction size distributions of granular filters: A numerical study. Geotechnique 2016;66:826–39. https://doi.org/10.1680/jgeot.15.P.215.

548 [15] Marot D, Rochim A, Nguyen HH, Bendahmane F, Sibille L. Assessing the susceptibility of
549 gap-graded soils to internal erosion: proposition of a new experimental methodology. Nat
550 Hazards 2016;83:365–88. https://doi.org/10.1007/s11069-016-2319-8.

551 [16] Liang J, Mohan S. Undrained fragility of clean sands, silty sands, and sandy silts. J Geotech
552 Geoenvironmental Eng 2002;128:849–59. https://doi.org/10.1061/jggefk.

553 [17] Shire T, O'Sullivan C, Hanley KJ. The influence of fines content and size-ratio on the micro-
554 scale properties of dense bimodal materials. Granul Matter 2016;18:1–10.
555 https://doi.org/10.1007/s10035-016-0654-9.

556 [18] Day RW, Thevanayagam S. Effect of fines and confining stress on undrained shear strength of
557 silty sands. J Geotech Geoenvironmental Eng 1999;125:1024–7.
558 https://doi.org/10.1061/(ASCE)1090-0241(1999)125:11(1024).

559 [19] Rahman MM, Lo SR, Baki MAL. Equivalent granular state parameter and undrained
560 behaviour of sand-fines mixtures. Acta Geotech 2011;6:183–94.
561 https://doi.org/10.1007/s11440-011-0145-4.

562 [20] Ke L, Takahashi A. Strength reduction of cohesionless soil due to internal erosion induced by
563 one-dimensional upward seepage flow. Soils Found 2012;52:698–711.
564 https://doi.org/10.1016/j.sandf.2012.07.010.

565 [21] Fonseca J, Sim WW, Shire T, O'Sullivan C, Wang Y, Dallo YAH. Microstructural analysis of
566 sands with varying degrees of internal stability. Geotechnique 2015;65:620–3.
567 https://doi.org/10.1680/geot.14.D.006.

568 [22] Moffat R, Herrera P. Hydromechanical model for internal erosion and its relationship with the
569 stress transmitted by the finer soil fraction. Acta Geotech 2015;10:643–50.
570 https://doi.org/10.1007/s11440-014-0326-z.

571 [23] Indraratna B, Israr J, Rujikiatkamjorn C. Geometrical method for evaluating the internal
572 instability of granular filters based on constriction size distribution. J Geotech
573 Geoenvironmental Eng 2015;141:1–14. https://doi.org/10.1061/(ASCE)GT.1943-
574 5606.0001343.

575 [24] Salot C, Gotteland P, Villard P. Influence of relative density on granular materials behavior:
576 DEM simulations of triaxial tests. Granul Matter 2009;11:221–36.
577 https://doi.org/10.1007/s10035-009-0138-2.

578 [25] ASTM D4253. Standard Test Methods for Maximum Index Density and Unit Weight of Soils
579 Using a Vibratory Table. ASTM Int West Conshohocken, PA 2014:1–15.
580 https://doi.org/10.1520/D4253-14.

581 [26] ASTM. ASTM D4254-00: Standard Test Methods for Minimum Index Density and Unit
582 Weight of Soils and Calculation of Relative Density. ASTM Stand 2006;I:9.
583 https://doi.org/10.1520/D4254-00R06E01.1.3.

584 [27] Monnet AG. Experiments on piping in sandy gravels. Geotechnique 1995;45:565–7.
585 https://doi.org/10.1680/geot.1995.45.3.565.

586 [28] Li M, Fannin RJ. A theoretical envelope for internal instability of cohesionless soil.
587 Geotechnique 2012;62:77–80. https://doi.org/10.1680/geot.10.T.019.

588 [29] Ahlinhan MF, Achmus M. Experimental investigation of critical hydraulic gradients for
589 unstable soils. Geotech Spec Publ 2010:599–608. https://doi.org/10.1061/41147(392)58.

590 [30] Kenney TC, Lau D. Internal stability of granular filters. Can Geotech J 1985;22:215–25.
591 https://doi.org/10.1139/t85-029.

592 [31] Mehdizadeh A, Disfani MM, Evans R, Arulrajah A. Impact of suffusion on the cyclic and

593 post-cyclic behaviour of an internally unstable soil. Geotech Lett 2019;9:218–24.
594 https://doi.org/10.1680/jgele.18.00128.

595 [32] Thevanayagam S, Mohan S. Intergranular state variables and stress-strain behaviour of silty
596 sands. Geotechnique 2000;50:1–23. https://doi.org/10.1680/geot.2000.50.1.1.

597 [33] Belhouari F, Bendani K, Missoum H, Derkaoui M. Undrained Static Response of Loose and
598 Medium Dense Silty Sand of Mostaganem (Northern Algeria). Arab J Sci Eng 2015;40:1327–
599 42. https://doi.org/10.1007/s13369-015-1629-6.

600 [34] Cundall PA, Strack ODL. A discrete numerical model for granular assemblies. Géotechnique
601 1979;29:47–65.

602 [35] Gong J, Nie Z, Zhu Y, Liang Z, Wang X. Exploring the effects of particle shape and content of
603 fines on the shear behavior of sand-fines mixtures via the DEM. Comput Geotech
604 2019;106:161–76. https://doi.org/10.1016/j.compgeo.2018.10.021.

605 [36] Farahnak Langroudi M, Soroush A, Tabatabaie Shourijeh P, Shafipour R. Stress transmission
606 in internally unstable gap-graded soils using discrete element modeling. Powder Technol
607 2013;247:161–71. https://doi.org/10.1016/j.powtec.2013.07.020.

608 [37] Farahnak Langroudi M, Soroush A, Shourijeh PT. A comparison of micromechanical
609 assessments with internal stability/instability criteria for soils. Powder Technol 2015;276:66–
610 79. https://doi.org/10.1016/j.powtec.2015.02.014.

611 [38] Minh NH, Cheng YP. A DEM investigation of the effect of particle-size distribution on one-
612 dimensional compression. Geotechnique 2013;63:44–53.
613 https://doi.org/10.1680/geot.10.P.058.

614 [39] Minh NH, Cheng YP, Thornton C. Strong force networks in granular mixtures. Granul Matter
615 2014;16:69–78. https://doi.org/10.1007/s10035-013-0455-3.

616 [40] Dai B, Yang J, Luo X. A numerical analysis of the shear behavior of granular soil with fines.
617 Particuology 2015;21:160–72. https://doi.org/10.1016/j.partic.2014.08.010.

618 [41] de Frias Lopez R, Ekblad J, Silfwerbrand J. Resilient properties of binary granular mixtures: A
619 numerical investigation. Comput Geotech 2016;76:222–33.
620 https://doi.org/10.1016/j.compgeo.2016.03.002.

621 [42] De Frias Lopez R, Silfwerbrand J, Jelagin D, Birgisson B. Force transmission and soil fabric
622 of binary granular mixtures. Geotechnique 2016;66:578–83.
623 https://doi.org/10.1680/jgeot.14.P.199.

624 [43] Gong J, Liu J. Mechanical transitional behavior of binary mixtures via DEM: Effect of
625 differences in contact-type friction coefficients. Comput Geotech 2017;85:1–14.
626 https://doi.org/10.1016/j.compgeo.2016.12.009.

627 [44] Garcia FE, Bray JD. Modeling the shear response of granular materials with discrete element
628 assemblages of sphere-clusters. Comput Geotech 2019;106:99–107.
629 https://doi.org/10.1016/j.compgeo.2018.10.003.

630 [45] Itasca Consulting Group I (2016) PFC3D 5.0 User Manual, Minneapolis n.d.

631 [46] Vaughan P. Soil mechanics MSc course notes: embankments and earthworks. London: 2006.

632 [47] Rs L. Preparing Test Specimens Using Undercompaction. Geotech Test J 1978;1:16–23.

633 [48] Reboul N, Vincens E, Cambou B. A statistical analysis of void size distribution in a simulated
634 narrowly graded packing of spheres. Granul Matter 2008;10:457–68. https://doi.org/DOI
635 10.1007/s10035-008-0111-5.

[49] Barreto D. Numerical and experimental investigation into the behaviour of granular materials under generalised stress states. Univ London 2009:357.

[50] Luis Alberto TC. Limit void ratios and steady-state line of non-plastic soils. Proc Inst Civ Eng Geotech Eng 2019;172:283–95. https://doi.org/10.1680/jgeen.18.00011.

[51] Lade P V., Liggio CD, Yamamuro JA. Effects of Non-Plastic Fines on Minimum and Maximum Void Ratios of Sand. Geotech Test J 1998;21:336–47. https://doi.org/10.1520/gtj11373j.

[52] Yang SL, Sandven R, Grande L. Instability of sand-silt mixtures. Soil Dyn Earthq Eng 2006;26:183–90. https://doi.org/10.1016/j.soildyn.2004.11.027.

[53] Park J, Santamarina JC. Revised Soil Classification System for Coarse-Fine Mixtures. J Geotech Geoenvironmental Eng 2017;143:1–13. https://doi.org/10.1061/(ASCE)GT.1943-5606.0001705.

[54] Andrianatrehina L, Souli H, Rech J, Taibi S, Fry JJ, Bunieski S, et al. Determination of the maximum diameter of free fines to assess the internal stability of coarse granular materials. Eur J Environ Civ Eng 2017;21:332–47. https://doi.org/10.1080/19648189.2015.1116468.

[55] Choo H, Burns SE. Shear wave velocity of granular mixtures of silica particles as a function of finer fraction, size ratios and void ratios. Granul Matter 2015;17:567–78. https://doi.org/10.1007/s10035-015-0580-2.

[56] Yin ZY, Huang HW, Hicher PY. Elastoplastic modeling of sand–silt mixtures. Soils Found 2016;56:520–32. https://doi.org/10.1016/j.sandf.2016.04.017.

[57] Chang CS, Meidani M, Deng Y. A compression model for sand–silt mixtures based on the concept of active and inactive voids. Acta Geotech 2017;12:1301–17. https://doi.org/10.1007/s11440-017-0598-1.

[58] Polito CP, Martin JR. Effects of nonplastic fines on the liquefaction resistance of sands. J Geotech Geoenvironmental Eng 2001;127:408–15. https://doi.org/10.1061/(ASCE)1090-0241(2001)127:5(408).

[59] Vallejo LE. Interpretation of the limits in shear strength in binary granular mixtures. Can Geotech J 2001;38:1097–104. https://doi.org/10.1139/cgj-38-5-1097.

[60] Kezdi A. Increase of protective capacity of flood control dikes. 1969.

[61] Crawford-Flett K. An improved hydromechanical understanding of seepage-induced instability phenomena in soil 2013:388.